PAPER

Antiferromagnetism induced by oxygen vacancies in V_2O_5 polycrystals synthesized by the Pechini method

IOP Publishing Journal of Physics D: Applied Physics
J. Phys. D: Appl. Phys. **48** (2015) 445002 (7pp) doi:10.1088/0022-3727/48/44/445002

Antiferromagnetism induced by oxygen vacancies in V_2O_5 polycrystals synthesized by the Pechini method

D Dreifus[1], M P F Godoy[1], A C Rabelo[2], A D Rodrigues[1], Y G Gobato[1], P C Camargo[1], E C Pereira[2] and A J A de Oliveira[1]

[1] Departamento de Física, Universidade Federal de São Carlos (UFSCar), CP 676, São Carlos, SP, Brazil
[2] Departamento de Química, Universidade Federal de São Carlos (UFSCar), CP 676, São Carlos, SP, Brazil

E-mail: adilson@df.ufscar.br

Received 23 April 2015
Accepted for publication 17 August 2015
Published 6 October 2015

Abstract

Optical and magnetic properties of V_2O_5 polycrystals were investigated through photoluminescence (PL) and magnetization measurements. The PL spectra comprise two main bands attributed to oxygen vacancies and to band-edge-related transitions. The magnetization measurements showed a predominant paramagnetic behavior in the temperature range studied (5 K–300 K) with a superimposed peak around 80 K associated with an antiferromagnetic phase. The temperature dependence of the magnetic results and the relative PL intensity presented a remarkable correlation while in the range of 80–200 K the intensity associated with oxygen vacancies became considerably more intense than band-to-band emissions, the same range in which the antiferromagnetic transition was observed. The observation of an antiferromagnetic phase in V_2O_5 was predicted in the literature although this result had not previously been measured experimentally. Raman spectroscopy was used as a complementary technique in order to exclude the presence of spurious vanadium oxide phases in the sample.

Keywords: vanadium pentoxide, antiferromagnetism, oxygen vacancies, optical properties, magnetic properties

(Some figures may appear in colour only in the online journal)

1. Introduction

Vanadium pentoxide (V_2O_5), in orthorhombic structure, has been widely used in a variety of scientific and technological applications due to its highly anisotropic electrical and optical properties making it a promising compound for applications such as high-capacity lithium batteries [1, 2], chemical sensors [3–5] and solar cells [3, 4]. The most exploited morphologies are polycrystals [6], nanofibers [5, 7], nanorods [8, 9], nanotubes [10, 11] and thin films [12–15].

In addition to many applications, oxides have also been widely studied due to their magnetic properties. In particular, a class of oxides with magnetic properties associated with the presence of structural defects caused by the insertion of dopants in the lattice or due to the thermal treatment used after the synthesis procedure, resulting in an increase or decrease of oxygen vacancies concentration in the samples studied. Among these oxides we can highlight Co and Ni doped ZnO [16, 17], Co and Mn doped TiO_2 [18–20], Fe doped SnO_2 [21, 22], In_2O_3 [23] and HfO_2 [24, 25]. The effects of oxygen-vacancies on the magnetic properties were observed particularly in CeO_2 [26].

The literature reports that orthorhombic V_2O_5 has a typical lamellar structure [4, 27, 28] in which vanadium atoms have no unpaired electrons in their last shell ($3d^0$) [29]. In other words, it was observed that V_2O_5 does not possess intrinsic magnetic moments and presents itself as a diamagnetic material [29]. However, in a study using spin density functional theory [30] it was calculated that changes in the atomic and the electronic structure, as well as in the magnetic properties

of V_2O_5 could be induced by oxygen deficiency in the structure, represented by V_2O_{5-x} by the authors. This analysis suggests that the higher the vacancy density, the greater the local distortion around vanadium atoms near the oxygen vacancies. The same authors also predict a ferromagnetic state present in the system for $x <$ ~0.13 and $0.19 < x <$ ~0.45, already reported in literature [31, 32], and an antiferromagnetic state ($0.45 \leqslant x \leqslant 0.5$), which was the object of study in this work. This behavior was never observed experimentally and is going to be discussed in this paper.

The aim of our work is to present the correlation between optical and magnetic properties observed in V_2O_5 polycrystals prepared by the Pechini method [33]. In our experimental study we observed that magnetic susceptibility shows a paramagnetic phase accompanied by a peak around 80 K characteristic of an antiferromagnetic transition. The photoluminescence spectra presented a band emission at lower energy associated with structural defects and another related to the band-edge emission. Furthermore, the optical band gap at 300 K was also estimated by diffuse reflectance spectroscopy as being 2.2 eV.

2. Experimental details

The V_2O_5 powder sample was synthesized by the Pechini method [33] as follows. NH_4VO_3 (M-P A Merck) was added to ethylene glycol (EG—P A Mallinckrodt) and the system was kept under constant stirring at 70 °C until complete dissolution. Afterwards citric acid (CA—P A Synth) was added to the solution, maintaining both temperature and stirring, until the compounds were completely dissolved. The material obtained was then polymerized at 110 °C (1 h), and calcined in two steps: one at 300 °C (2 h) and another at 550 °C (4 h). After the calcination process the powder obtained was macerated.

The morphology and the microstructure of the V_2O_5 powder was investigated using scanning electron microscopy (FEG-SEM) and x-ray diffraction (XRD) with Cu K_α radiation at a wavelength of 1.54 Å. The 2θ scan was performed from 10° to 110° with 0.02° increments and the XRD data were analyzed by the Rietveld refinement method [34] using GSA/EXPGUI [35, 36] software. Raman spectroscopy was used as a complementary structural determination. The measurement was accomplished using a triple grating spectrometer equipped with microscope facilities. The experimental configurations were adjusted to provide a spectral resolution of 1.5 cm^{-1}. The line 488 nm of an argon laser was used as an excitation source with controlled power in order to avoid heating effects.

The sample was also characterized by diffuse reflectance spectroscopy (DRS) for band gap energy determination. Additional optical properties were investigated using photoluminescence spectroscopy technique as a function of the temperature in the range 15–300 K. For optical excitation, we employed the 325 nm line from a He–Cd laser. The V_2O_5 optical emission was monitored by an Ocean Optics spectrometer model (USB4000-UV–Vis / 200 μm slit) in the range 350–1000 nm.

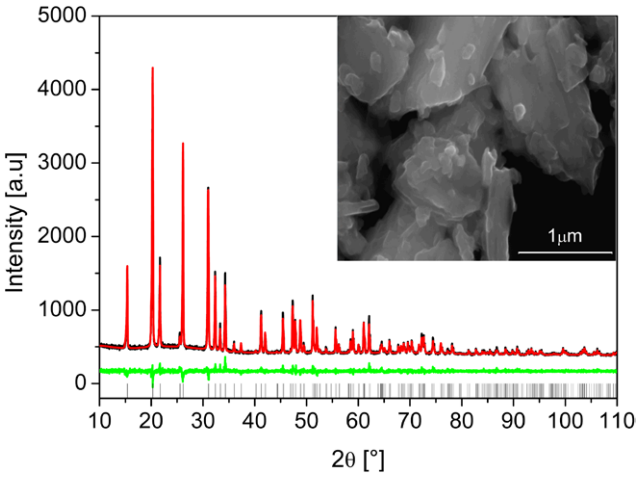

Figure 1. Room temperature XRD pattern for V_2O_5 polycrystals. The black line indicates observed collected data (Y_{Obs}), the red line refers to calculated data (Y_{Calc}) by the Rietveld refinement method and the green line shows the difference between observed and calculated data. The black bars correspond to Bragg peaks of V_2O_5 orthorhombic phase.

Magnetization as a function of applied magnetic field, up to 70 kOe, and magnetic susceptibility as a function of temperature (1.8–300 K) measurements, using zero field cooled (ZFC) and field cooled (FC) protocols were performed using a SQUID-VSM magnetometer (MPMS®3—Quantum Design).

3. Results and discussion

3.1. Structural and morphological properties

XRD measurements performed at room temperature characterized the sample as being orthorhombic V_2O_5 (ICSD Code: 60767), spatial group Pmmn. Presenting the following lattice parameters: $a = 11.514(0)$ Å, $b = 3.565(2)$ Å, $c = 4.374(7)$ Å, $\alpha = \beta = \gamma = 90°$. The Rietveld quality factors showed conformity between experimental data and the fitted curve as follows: $R_{WP} = 0.106$ and $\chi^2 = 1.39$. Figure 1 also confirms the good data fitting between the calculated profile (Y_{Cal}) and the observed profile (Y_{Obs}). In the inset presented in figure 1, the lamellar morphology expected for V_2O_5 is also confirmed by FEG-SEM images.

In order to rule out the possibility of the presence of a spurious phase in the sample we performed a Raman spectroscopy measurement at 300 K which is presented in figure 2. The peaks are typical of the orthorhombic structure of V_2O_5, belonging to spatial group Pmmn (D^{13}_{2h}) [37]. The spectrum presents no peaks which can be related to other types of common vanadium oxide structures, such as VO_2 or V_2O_3 [38, 39].

3.2. Optical properties

Several methods have been developed and applied to derive band gap energy (E_g) values of semiconductors including optical absorption and DRS. In this work, we have used Kubelka–Munk theory [40, 41] into DRS data to determine

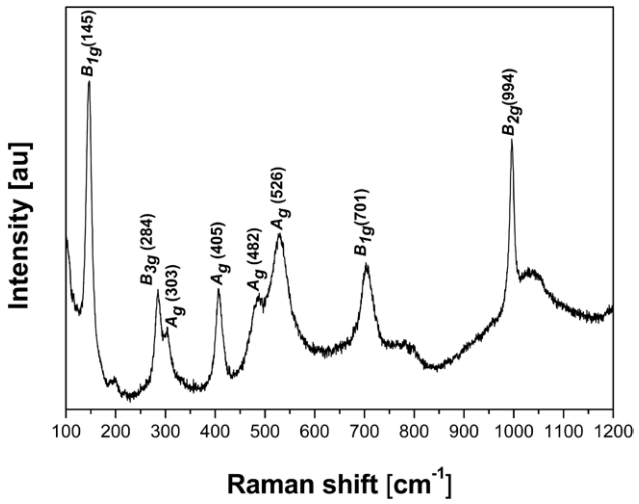

Figure 2. Room temperature Raman spectrum of orthorhombic V_2O_5, collected at 300 K. Peaks are assigned with their spatial symmetries and corresponding wave numbers in cm^{-1} units.

the E_g in a V_2O_5 sample at room temperature. This model holds when the diffuse reflection no longer allows one to separate the contributions of the reflection, refraction and diffraction (i.e. scattering occurs). In the parabolic band-structure approximation, E_g and linear absorption coefficient α of a semiconductor are related through the equation (1) [42]:

$$\alpha h\upsilon = C_1(h\upsilon - E_g)^n \quad (1)$$

where $h\upsilon$ is the photon energy, C_1 is a proportionality constant, n could be 2, 3, 1/2 and 3/2 for indirect allowed, indirect forbidden, direct allowed and direct forbidden transitions [43, 44], respectively. The n value for the specific transition can be determined by the best linear fit in the lower absorption region [10, 11]. In the case of materials that scatter in perfectly diffuse manner we can write [45]:

$$[F(R_\infty)h\upsilon]^{\frac{1}{n}} = C_2(c - E_g) \quad (2)$$

$F(R_\infty)$ is directly related to K/S where **S** and **K** are the so-called K–M [45] scattering and absorption coefficients, respectively. Therefore, obtaining $F(R_\infty)$ from equation (2) and plotting $[F(R_\infty)h\upsilon]^{\frac{1}{n}}$ against $h\upsilon$, the E_g of a powder sample can be extracted easily as shown in figure 3. For our sample, n equals 2, a typical value for an indirect band gap in accordance with theoretical band calculation [45] and with single crystal experimental data for V_2O_5 [46].

Our optical band gap estimative at room temperature for V_2O_5 was 2.2 eV, in agreement with results found by other authors [13, 14, 47, 48]. It should be noted that variations in the band gap energy may be related to the degree of nonstoichiometry in V_2O_5 [49].

In order to study the PL properties of V_2O_5, the powder was compressed into a tablet with 5 mm diameter. The PL emission spectra were investigated as a function of the temperature from 15 K up to 300 K. Figure 4 shows typical PL spectra for the V_2O_5 sample for different temperatures.

Two broad band emissions were observed at 15 K, a lower energy band centered at 1.76 eV (~700 nm) and a broader band

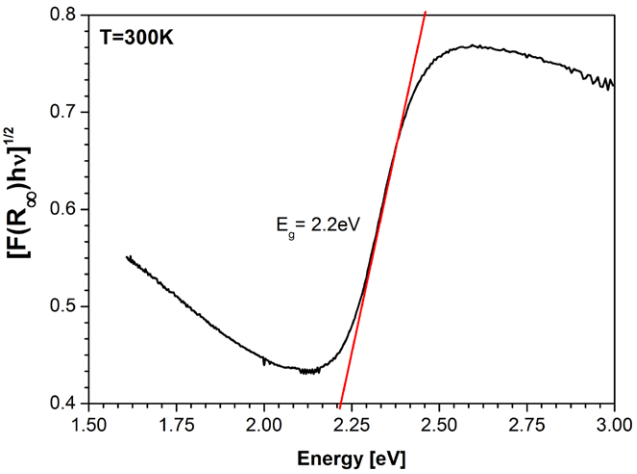

Figure 3. Kubelka–Munk transformed reflectance spectra as a function of energy at room temperature for the V_2O_5 sample.

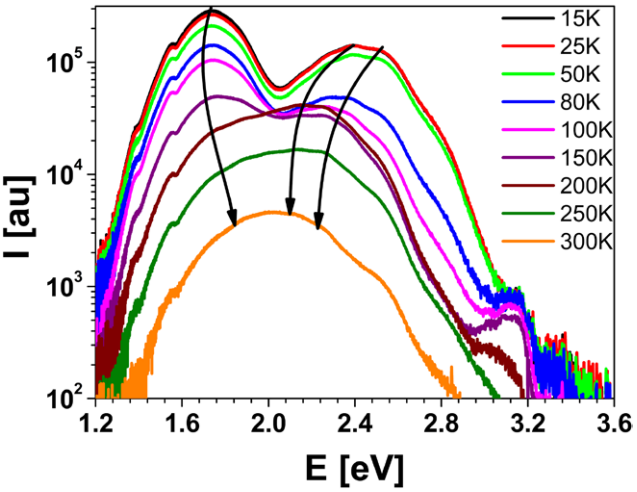

Figure 4. Logarithm of PL intensity as a function of energy for the V_2O_5 sample. The black arrows indicate the emission peak energy evolution as the temperature is increased.

at 2.4 eV (~515 nm). It was observed that the relative intensity of both bands is very sensitive to the temperature changes as illustrated in figure 4.

The V_2O_5 band gap was previously reported in the range 2.15–2.65 eV due to indirect and direct gaps [50]. At 300 K our results show both emissions, one at 2.2 eV associated to indirect band gap, as observed in DRS experiments, and a higher energy peak that can be attributed to the direct band gap [50]. When the temperature increases from 15 to 300 K, this band has a red shift as expected for band gap transitions due to semiconductors [51]. Therefore we attribute this broader band to band-edge transitions of V_2O_5 powder.

On the other hand the band at lower energy might be attributed to defects such as oxygen vacancies (V_O) [52, 53] introduced during synthesis and calcination processes. V_O plays an important role in the electrical and optical properties of semiconductor oxides introducing localized energy levels in the band gap. As a consequence, when the energy separation between these localized levels and conduction (and/or valence) bands is in the order of the thermal energy,

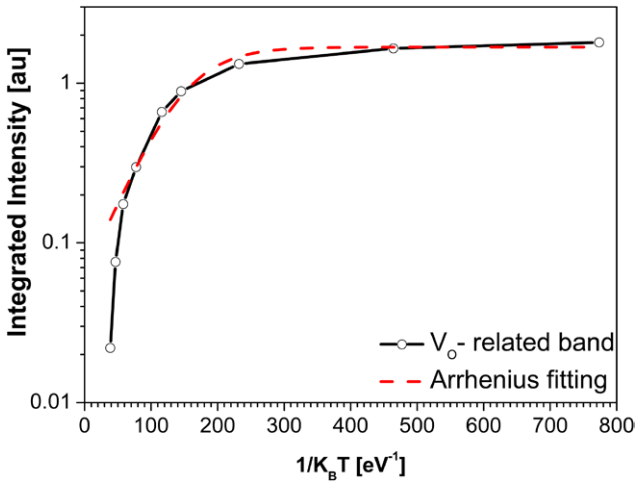

Figure 5. Integrated PL intensity as a function of reciprocal thermal energy and the Arrhenius fit curve for the vacancy-related band emission.

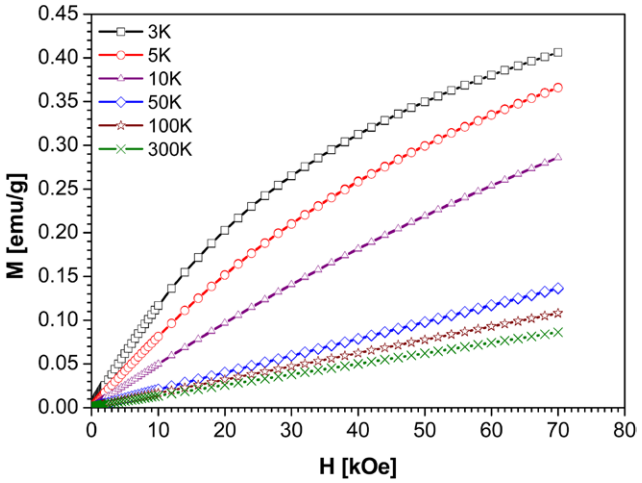

Figure 6. Magnetization (M) as a function of the applied magnetic field (H) for V_2O_5 polycrystals in the temperature range of 3–300 K. The paramagnetic behavior is observed in the whole temperature range.

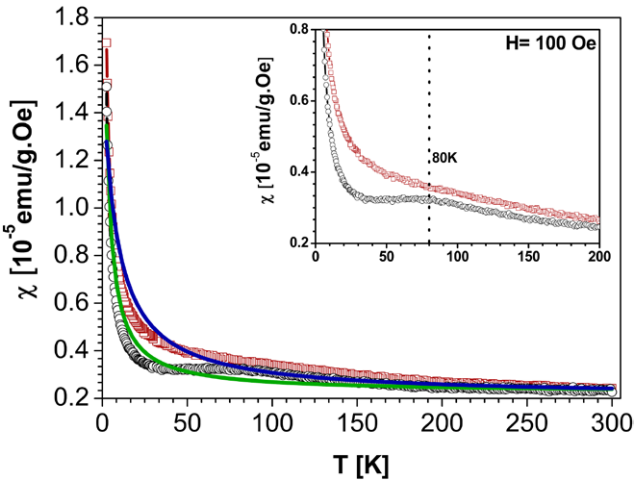

Figure 7. Magnetic susceptibility (χ) versus temperature (T) at $H = 100$ Oe for V_2O_5 polycrystals. Black circles and red squares correspond to ZFC and FC curves, respectively. The inset shows in detail a broad peak in 80 K associated with an antiferromagnetic contribution. The green and blue lines are the Curie–Weiss fitting for the ZFC and FC curves, respectively.

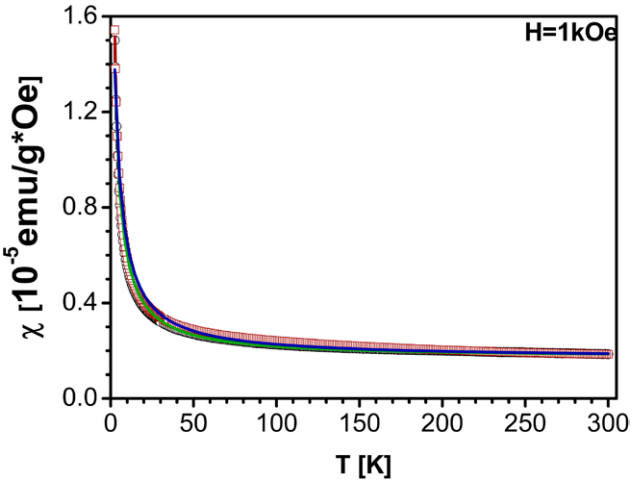

Figure 8. Magnetic susceptibility (χ) versus temperature (T) at $H = 1$ kOe for V_2O_5 polycrystals. Black circles and red squares correspond to ZFC and FC curves, respectively. At this field the broad peak at 80 K associated with an antiferromagnetic contribution and the thermal irreversibility are not observed.

charge carriers can be promoted to the conduction band (or trapped from the valence band) contributing to an increase in the electrical conductivity. For optical emissions these levels can also work as a new channel of recombination giving origin to donor–acceptor or vacancy-related emissions. This is the case observed in many oxide systems with nonstoichiometric contents of oxygen like ZnO, SnO_2 and In_2O_3 [54–56]. As the temperature is increased the vacancy-related band shows a slight blue shift compared to band-edge emissions (figure 4).

It is important to note that the ratio between the intensities of the two broad band changes at 80 K. At this temperature the band-edge emission and the vacancy-related emission present the same intensity. As the temperature is increased the vacancy-related emission becomes more intense than the band-edge emission up to approximately 200 K. This means that, for electrons in conduction band carriers relaxation to vacancy-related levels are more favorable than radioactive recombinations by band-to-band processes. Above 200 K, the intensity of the V_O-related band starts to decrease drastically compared to band-edge emissions. At room temperature the spectrum shows a convoluted emission from the two bands.

In order to investigate the activation energy of vacancy-related band emission, we have analyzed the integrated PL intensity as a function of reciprocal temperature (figure 5) using the Arrhenius equation:

$$I(T) = \frac{I_0}{1 + \gamma e^{-\frac{E_{at}}{k_b T}}} \tag{3}$$

where k_B is the Boltzmann constant, I_0 is the PL intensity at 0 K, γ is the ratio between radioactive and non-radioactive lifetimes and E_{at} is an activation energy. The fitted parameters for the V_O-related band are $I_0 = (1.68 \pm 0.07)$ au, $\gamma = 26 \pm 11$ and $E_{at} = (22 \pm 3)$ meV. This activation energy means that

Table 1. Values obtained after Curie–Weiss fitting to the magnetic susceptibility as a function of temperature data for 100 Oe and 1000 Oe.

	ZFC curve			FC curve		
H (Oe)	C (emu.K (g.Oe)$^{-1}$)	θ (K)	χ_0 (emu (g.Oe)$^{-1}$)	C (emu.K (g.Oe)$^{-1}$)	θ (K)	χ_0 (emu (g.Oe)$^{-1}$)
100	4.0E−5	−1.5	2.2E−6	4.9E−5	−0.8	2.3E−6
1000	5.0E−5	−1.6	1.7E−6	6.0E−5	−2.5	1.7E−6

thermal energy is sufficient to avoid carriers being trapped in vacancy-related levels or otherwise ionize these vacancies in such a way that electrons are promoted to the conduction band above 258 K.

3.3. Magnetic properties

In figure 6 we present magnetization as a function of the applied magnetic field for V_2O_5 polycrystals. The system exhibits a paramagnetic behavior in the whole temperature range without a significant coercive field at 3 K.

On the other hand, magnetic susceptibility measurements ($\chi = M/H$) as a function of temperature performed with an applied field of $H = 100$ Oe, using ZFC and FC protocol, as showed in figure 7, presented a thermal irreversibility associated with the ZFC/FC processes below 80 K. At this temperature the ZFC curve exhibits a broad peak associated to an antiferromagnetic transition, in addition to the paramagnetic behavior observed within the whole temperature range.

When the applied magnetic field is increased to $H = 1$ kOe, as shown in figure 8, the peak at 80 K vanishes and the thermal irreversibility is no longer observed suggesting a weak antiferromagnetic interaction.

The evidence of the association of the peak at 80 K with an antiferromagnetic phase transition is based on the data presented in table 1. The well-known Curie–Weiss fitting was applied in magnetic susceptibility data using the equation $\chi = C/(T - \theta) + \chi_0$, where C is the Curie constant, T is the temperature, θ determines the type of interaction between the moments and χ_0 is an additional constant related to a susceptibility which is temperature independent.

The data obtained after the fit confirms the presence of an antiferromagnetic interaction in the system represented by negative values of θ. C is related to the number of magnetic moments and one can see that it has the same order of magnitude (10^{-5}emu.K (g.Oe)$^{-1}$) in all curves for the entire temperature range studied. χ_0 is related to an intrinsic susceptibility of the system, i.e. it is not directly related to the magnetic moments due to defects and is constant, around 10^{-6} emu (g.Oe)$^{-1}$.

According to Zimmermann *et al* [29] in its single-phase form V_2O_5 is a diamagnetic material, however, an orbital hybridization due to the strong coupling between the V 3d and the O 2p ligand orbitals could lead to a spin distribution and consequently a magnetic phase as observed in this work. Density functional theory (DFT) analysis [30] predicted that the oxygen vacancies present in V_2O_{5-x} samples would induce changes in its atomic and electronic structure, as well as in its magnetic properties. The DFT calculations showed that for $x < 0.13$ and $0.19 < x < 0.45$ the system would present a ferromagnetic ordering, however, for $0.45 \leqslant x \leqslant 0.5$ there would be an antiferromagnetic ordering in V_2O_{5-x}. The peak observed in magnetic susceptibility as a function of temperature, as shown in figure 7, is evidence of antiferromagnetic interaction. In that work, the authors also claim that for oxygen deficiencies as large as $x \sim 0.5$, the V_2O_{5-x} crystalline structure changes from orthorhombic to monoclinic. As verified by XRD (figure 1) and confirmed by Raman spectroscopy analysis (figure 2), our sample consists exclusively orthorhombic V_2O_5 leading to the conclusion that oxygen vacancy density in our sample is not large enough to cause structural changes as suggested by Xiao and Guo [30] but enough to produce the magnetic properties observed.

The alternative model for explaining the magnetic behavior observed in our magnetic susceptibility measurements was proposed by Kaminski and Das Sarma [57] and is based on the formation of bounded magnetic polarons, due to the interaction between localized holes and impurities, which causes spontaneous magnetization in diluted magnetic semiconductors. In our case, at low temperatures, the V_2O_5 sample reaches a state where the spins have an antiferromagnetic impurity-hole exchange interaction [58–60]. Comparing the defects band emission intensity data with the band-edge emission intensity data, from 80 K to 200 K (figure 4), we observed that as the temperature decreases the emission related to oxygen vacancies becomes larger than the emission due to the band-edge recombinations. This effect might be related to the growth of the effective radius of the magnetic polarons as the temperature is lowered, as calculated by Kaminski and Das Sarma [57], and gives origin to the antiferromagnetic behavior observed in the sample. However, the largest part of the polarons in the sample is not coupled antiferromagnetically and the system presents a predominance of paramagnetic behavior.

4. Conclusions

In this work we investigated the relation between oxygen vacancies present in V_2O_5 polycrystals, obtained by the Pechini method after a calcination at 550 °C during 4 h, and their structural, optical and magnetic properties. The Rietveld refinement of the XRD and Raman spectra analysis confirmed the presence of a single orthorhombic V_2O_5 phase in the sample. FEG-SEM images showed that V_2O_5 presents a lamellar structure and DRS measurements estimated the optical band gap as being 2.2 eV at 300 K.

Comparing the magnetic measurement data to photoluminescence measurements as a function of temperature we observed a correlation between the vacancies of oxygen and the magnetic properties, as expected by theoretical predictions.

In the 5–300 K temperature range a paramagnetic behavior is accompanied by a peak centered at 80 K characteristic of an antiferromagnetic transition. In addition, the defect associated band emission intensity is higher than the band gap emission intensity from 80 K to 200 K, the same region where the antiferromagnetic peak has been observed. Thus we suppose that this effect is connected to the growth of the effective radius of the magnetic polarons which mediate the antiferromagnetic interaction observed as the temperature is lowered.

Since V_2O_5 is widely known for its unusual electronic and optical properties, understanding the relation between its magnetic and optical properties due to the structural defects present in the sample, caused by the synthesis technique used, opens the possibility of developing versatile devices.

Acknowledgments

The authors acknowledge the scientific support of FAPESP (grants 2013/17657-2, 2013/07296-2 and 2012/24025-0), CAPES and CNPq.

References

[1] Kosacki I, Massot M, Balkanski M and Tuller H L 1992 Electrical conductivity and Raman scattering of amorphous V_2O_5–$LiBO_2$ *Mater. Sci. Eng.* B **12** 345–9
[2] Nomura Y S T, Tanaka H and Kobayakawa K 1991 Charge/discharge characteristics of electrolytically prepared V_2O_5 as a cathode active material of lithium secondary battery *J. Electrochem. Soc.* **138** L37
[3] Schönauer-Kamin D, Fleischer M and Moos R 2014 Influence of the V_2O_5 content of the catalyst layer of a non-Nernstian NH_3 sensor *Solid State Ion.* **262** 270–3
[4] Raible I, Burghard M, Schlecht U, Yasuda A and Vossmeyer T 2005 V_2O_5 nanofibres: novel gas sensors with extremely high sensitivity and selectivity to amines *Sensors Actuators* B **106** 730–5
[5] Modafferi V, Trocino S, Donato A, Panzera G and Neri G 2013 Electrospun V_2O_5 composite fibers: synthesis, characterization and ammonia sensing properties *Thin Solid Films* **548** 689–94
[6] Gotić M, Popović S, Ivanda M and Musić S 2003 Sol–gel synthesis and characterization of V_2O_5 powders *Mater. Lett.* **57** 3186–92
[7] Kim G T, Muster J, Krstic V, Park J G, Park Y W, Roth S and Burghard M 2000 Field-effect transistor made of individual V_2O_5 nanofibers *Appl. Phys. Lett.* **76** 1875
[8] Hu Y, Li Z, Zhang Z and Meng D 2009 Effect of magnetic field on the visible light emission of V_2O_5 nanorods *Appl. Phys. Lett.* **94** 103107
[9] Wang Y, Li Z, Sheng X and Zhang Z 2007 Synthesis and optical properties of V_2O_5 nanorods *J. Chem. Phys.* **126** 164701
[10] Petkov V, Zavalij P Y, Lutta S, Whittingham M S, Parvanov V and Shastri S 2004 Structure beyond Bragg: study of V_2O_5 nanotubes *Phys. Rev.* B **69** 085410
[11] Demishev S V *et al* 2011 Magnetic properties of vanadium oxide nanotubes and nanolayers *Phys. Rev.* B **84** 094426
[12] Acharya B S and Nayak B B 2008 Microstructural studies of nanocrystalline thin films of V_2O_5–MoO_3 using x-ray diffraction, optical absorption and laser micro Raman spectroscopy *Indian J. Pure Appl. Phys.* **46** 866–75
[13] Benmoussa M 1995 Structural, electrical and optical properties of sputtered vanadium pentoxide thin films *Thin Solid Films* **265** 22–8
[14] Benmoussa M, Outzourhit A, Jourdani R and Bennouna A 2003 Structural, optical and electrochromic properties of sol–gel V_2O_5 thin films *Act. Passive Electron. Compon.* **26** 245–56
[15] Kang M, Oh E, Kim I, Kim S W, Ryu J W and Kim Y G 2012 Optical characteristics of amorphous V_2O_5 thin films colored by an excimer laser *Curr. Appl. Phys.* **12** 489–93
[16] Balti I, Mezni A, Dakhlaoui-Omrani A, Léone P, Viana B, Brinza O, Smiri L-S and Jouini N 2011 Comparative study of Ni- and Co-substituted ZnO nanoparticles: synthesis, optical, and magnetic properties *J. Phys. Chem.* C **115** 15758–66
[17] Sudakar C, Kharel P, Lawes G, Suryanarayanan R, Naik R and Naik V M 2007 Raman spectroscopic studies of oxygen defects in Co-doped ZnO films exhibiting room-temperature ferromagnetism *J. Phys.: Condens. Matter* **19** 026212
[18] Serrano A *et al* 2009 Room-temperature ferromagnetism in the mixtures of the TiO_2 and Co_3O_4 powders *Phys. Rev.* B **79** 144405
[19] Karthik K, Pandian S K, Kumar K S and Jaya N V 2010 Influence of dopant level on structural, optical and magnetic properties of Co-doped anatase TiO_2 nanoparticles *Appl. Surf. Sci.* **256** 4757–60
[20] Xu L M, Yu Y P, Xing X J, Wu X Y and Li S W 2008 Enhancement of ferromagnetism upon thermal annealing in plasma assisted MBE grown mixed-phase Mn-doped insulating TiO_2 thin films *Appl. Phys.* A **92** 361–5
[21] Fitzgerald C, Venkatesan M, Dorneles L, Gunning R, Stamenov P, Coey J, Stampe P, Kennedy R, Moreira E and Sias U 2006 Magnetism in dilute magnetic oxide thin films based on SnO_2 *Phys. Rev.* B **74** 115307
[22] Rodríguez Torres C E, Errico L, Golmar F, Mudarra Navarro A M, Cabrera A F, Duhalde S, Sánchez F H and Weissmann M 2007 The role of the dopant in the magnetism of Fe-doped SnO_2 films *J. Magn. Magn. Mater.* **316** e219–22
[23] Panguluri R P, Kharel P, Sudakar C, Naik R, Suryanarayanan R, Naik V M, Petukhov A G, Nadgorny B and Lawes G 2009 Ferromagnetism and spin-polarized charge carriers in In_2O_3 thin films *Phys. Rev.* B **79** 165208
[24] Beltrán J I, Muñoz M C and Hafner J 2008 Structural, electronic and magnetic properties of the surfaces of tetragonal and cubic HfO_2 *New J. Phys.* **10** 063031
[25] Coey J M D 2005 D0 ferromagnetism *Solid State Sci.* **7** 660–7
[26] Fernandes V *et al* 2009 Dilute-defect magnetism: origin of magnetism in nanocrystalline CeO_2 *Phys. Rev.* B **80** 035202
[27] Modafferi V, Panzera G, Donato A, Antonucci P L, Cannilla C, Donato N, Spadaro D and Neri G 2012 Highly sensitive ammonia resistive sensor based on electrospun V_2O_5 fibers *Sensors Actuators* B **163** 61–8
[28] Aita C R, Liu Y, Mei L K and Hansen S D 1986 Optical behavior of sputter-deposited vanadium pentoxide *J. Appl. Phys.* **60** 749
[29] Zimmermann R, Claessen R, Reinert F, Steiner P and Hüfner S 1998 Strong hybridization in vanadium oxides: evidence from photoemission and absorption spectroscopy *J. Phys.: Condens. Matter* **10** 5697–716
[30] Xiao Z R and Guo G Y 2009 Structural, electronic and magnetic properties of V_2O_{5-x}: an *ab initio* study *J. Chem. Phys.* **130** 214704
[31] Cezar A B, Graff I L, Varalda J, Schreiner W H and Mosca D H 2014 Oxygen-vacancy-induced room-temperature magnetization in lamellar V_2O_5 thin films *J. Appl. Phys.* **116** 163904

[32] Xiao Z R, Guo G Y, Lee P H, Hsu H S and Huang J C A 2008 Oxygen vacancy induced ferromagnetism in V_2O_{5-x} *J. Phys. Soc. Japan* **77** 23706
[33] Pechini M P 1967 *US Patent* No 3.330.697
[34] Young R A 1999 *The Rietveld Method* (*Oxford Science Publications*) (Oxford: Oxford University Press)
[35] Larson A C and Von-Dreele R B 2000 General structure analysis system (GSAS) *Los Alamos Natl. Lab. Rep. LAUR* 86–748
[36] Toby B H 2001 EXPGUI, a graphical user interface for GSAS *J. Appl. Cryst.* **34** 210–3
[37] Piccirillo C, Binions R and Parkin I 2007 Synthesis and functional properties of vanadium oxides: V_2O_3, VO_2, and V_2O_5 deposited on glass by aerosol-assisted CVD *Chem. Vapor Depos.* **13** 145–51
[38] Petrov G I, Yakovlev V V and Squier J 2002 Raman microscopy analysis of phase transformation mechanisms in vanadium dioxide *Appl. Phys. Lett.* **81** 1023
[39] Tatsuyama C and Fan H Y 1980 Raman scattering and phase transitions in V_2O_3 and $(V_{1-x}Cr)_2O_3$ *Phys. Rev.* B **21** 2977–83
[40] Kubelka P and Munk F 1931 Ein beitrag zur optik der farbanstriche *Z. Tech. Phys* **12** 593–601
[41] Tolvaj L, Mitsui K and Varga D 2011 Validity limits of Kubelka − Munk theory for DRIFT spectra of photodegraded solid wood *Wood Sci. Technol.* **45** 135–46
[42] Smith R A 1978 *Semiconductors* (Cambridge: Cambridge University Press)
[43] Hossein A A, Hogarth C A and Beynon J 1994 Optical absorption in CeO_2–V_2O_5 evaporated thin films *J. Mater. Sci. Lett.* **13** 1144–5
[44] Khan G A and Hogarth C A 1991 Electron spin resonance studies of evaporated V_2O_5 and co-evaporated V_2O_5/B_2O_3 thin films *J. Mater. Sci.* **26** 2707–10
[45] Escobedo Morales A, Sánchez Mora E and Pal U 2007 Use of diffuse reflectance spectroscopy for optical characterization of un-supported nanostructures *Rev. Mex. Fis. S* **53** 18–22
[46] Parker J C, Lam D J, Xu Y-N and Ching W Y 1990 Optical properties of vanadium pentoxide determined from ellipsometry and band-structure calculations *Phys. Rev.* B **42** 5289
[47] Eyert V and Höck K-H 1998 Electronic structure of V_2O_5: role of octahedral deformations *Phys. Rev.* B **57** 12727–37
[48] Talledo A and Granqvist C G 1995 Electrochromic vanadium-pentoxide-based films: structural, electrochemical, and optical properties *J. Appl. Phys.* **77** 4655–66
[49] Moshfegh A Z and Ignatiev A 1991 Formation and characterization of thin film vanadium oxides: auger electron spectroscopy, x-ray photoelectron spectroscopy, x-ray diffraction, scanning electron microscopy, and optical reflectance studies *Thin Solid Films* **198** 251–68
[50] Manil K, Sok Won K, Younghun H, Youngho U and Ji-Wook R 2013 Temperature dependence of the interband transition in a V_2O_5 film *AIP Adv.* **3** 052129
[51] Varshni Y P 1967 Temperature dependence of the energy gap in semiconductors *Physica* **34** 149–54
[52] Hong N H, Sakai J, Poirot N and Brizé V 2006 Room-temperature ferromagnetism observed in undoped semiconducting and insulating oxide thin films *Phys. Rev.* B **73** 132404
[53] Yoon S D, Chen Y, Yang A, Goodrich T L, Zuo X, Arena D A, Ziemer K, Vittoria C and Harris V G 2006 Oxygen-defect-induced magnetism to 880 K in semiconducting anatase TiO_2—δ films *J. Phys.: Condens. Matter* **18** L355–61
[54] Vanheusden K, Seager C H, Warren W L, Tallant D R and Voigt J A 1996 Correlation between photoluminescence and oxygen vacancies in ZnO phosphors *Appl. Phys. Lett.* **68** 403
[55] Luo S H, Fan J Y, Liu W L, Zhang M, Song Z T, Lin C L, Wu X L and Chu P K 2006 Synthesis and low-temperature photoluminescence properties of SnO_2 nanowires and nanobelts *Nanotechnology* **17** 1695
[56] Peng X S, Meng G W, Zhang J, Wang X F, Wang Y W, Wang C Z and Zhang L D 2002 Synthesis and photoluminescence of single-crystalline In_2O_3 nanowires *J. Mater. Chem.* **12** 1602–5
[57] Kaminski A and Das Sarma S 2002 Polaron percolation in diluted magnetic semiconductors *Phys. Rev. Lett.* **88** 247202
[58] Pantelides S T 1978 The electronic structure of impurities and other point defects in semiconductors *Rev. Mod. Phys.* **50** 797–858
[59] Dietl T and Spalek J 1982 Effect of fluctuation of magnetization on the bound magnetic polaron: comparsion with experiment *Phys. Rev. Lett.* **48** 355
[60] Wolff P A, Bhatt R N and Durst A C 1996 Polaron–polaron interactions in diluted magnetic semiconductors *J. Appl. Phys.* **79** 5196